Supplementary Information

Atomic tuning of 3D printed carbon surface chemistry for electrocatalytic nitrite oxidation and reduction to ammonia

Wanli Gao[a], Jan Michalička[b], and Martin Pumera[a,c,d]*

[a]Future Energy and Innovation Laboratory, Central European Institute of Technology, Brno University of Technology, Purkyňova 123, 61200 Brno, Czech Republic

[b]Central European Institute of Technology, Brno University of Technology, Purkyňova 123, 61200 Brno, Czech Republic

[c]Faculty of Electrical Engineering and Computer Science, VSB - Technical University of Ostrava, 17. listopadu 2172/15, 70800 Ostrava, Czech Republic

[d]Department of Medical Research, China Medical University Hospital, China Medical University, No. 91 Hsueh-Shih Road, Taichung 40402, Taiwan

E-mail: martin.pumera@ceitec.vutbr.cz

Ti content determination by inductively coupled plasma optical emission spectrometry (ICP-OES)

Before ICP-OES measurement, the 1D@TiO_2 electrode had to be dissolved using a microwave digestion procedure. The electrode was accurately weighed on a microbalance (Radwag MYA 5.6.Y) and placed in a teflon tube. A reaction mixture consisting of 2 ml HNO_3, 2 ml H_2O_2, 5 ml $HClO_4$ and 1 ml HF (all Analpure grade, Analytika s r.o., Czech Republic) was added and the tube was placed in a microwave digestion unit (Magnum II, Ertec, Poland). After 30 minutes of four-step digestion procedure utilizing limits up to 300 °C and 42 bar, the samples were transferred into plastic tubes, diluted with demineralized water and spiked with yttrium (serving as internal standard) solution (Analytika s r.o., Czech Republic) to obtain final Y concentration 2 mg/l. The samples were subsequently analyzed by ICP-OES with a radial view of the plasma (Arcos MV, Spectro, Germany). An external calibration in the range 0 - 10 mg/l Ti and Fe with 2 mg/l Y as an internal standard was used. Certified standard solutions Ti and Fe (multielemental, 100 mg/l each) and Y (1000 mg/l) from Analytika s r.o., Czech Republic, nitric acid (Analpure grade, Analytika s r.o., Czech Republic) and demineralized water were used to prepare the calibration solutions.

Differential scanning calorimetry (DSC)

DSC measurements were conducted using the DSC600 Thermal Analysis System (HITACHI) under a nitrogen atmosphere. Samples with a mass of ~ 3 mg were used for each DSC measurement. Each sample was heated from 20 °C to 210 °C at a heating rate of 10 °C/min to obtain the melting curve. The Fusion enthalpy and cold crystallization enthalpy (if exists) will be used to calculate the crystallinity degree of PLA [1]. The degree of crystallinity (X_c) of PLA is calculated by the following equation:

$$X_c = \frac{\Delta H_f - \Delta H_{fc}}{\phi H_f^*} \times 100\ \%$$

where ϕ is the weight fraction of PLA in the 3D-printed nanocarbon frameworks (around 86 %), ΔH_f is fusion enthalpy, ΔH_{fc} is cold crystallization enthalpy, and H_f^* is the fusion enthalpy of 100% crystalline PLA (93 J g^{-1}).

Calculation of electrochemically active surface area (ECSA):

To determine the electrochemical double-layer capacitance (C_{DL}), cyclic voltammetry was conducted in a non-Faradaic potential range at different scan rates. The double-layer current (i_{DL}), scan rate (v), and C_{DL} exhibit a linear relationship of $i_{DL} = vC_{DL}$. The value of C_{DL} can be obtained from the slop of i_{DL} plotted against v. The average of the absolute values of the anodic and cathodic slopes is used as C_{DL}. The ECSA was then calculated using the equation $ECSA = C_{DL} / C_s$, where C_s = 22 μF cm^{-2} is for the specific capacitance of the carbon material [2].

Calculation of NH_3 yield rate and the Faradaic efficiency (FE):

The NH_3 yield rate (r_{NH_3}) and FE were calculated using the following equations:

$$r_{NH_3} = (17 c_{NH_3} \times V) / (t \times S)$$

$$FE = (8F \times c_{NH_3} \times V) / Q$$

where c_{NH_3} is the concentration of measured NH_3, V is the electrolyte volume of the cathodic compartment, t is the reaction time, S is the geometric area of working electrode, F is the Faradaic constant (96485 C mol^{-1}), and Q is the total charge passing the electrode.

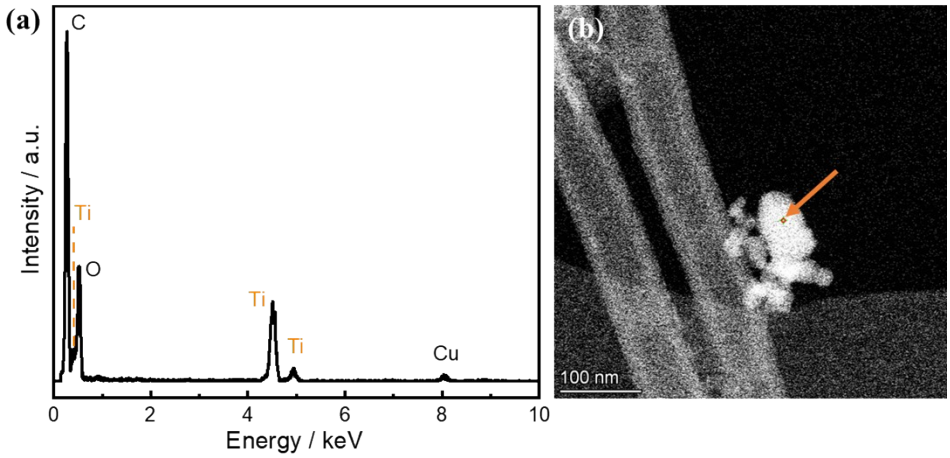

Figure S1. (a) STEM-EDX point spectrum marked by the arrow in the image of (b), showing that the Ti-based impurities exist on the surface of the carbon nanotube. The Cu signal is from the TEM grid.

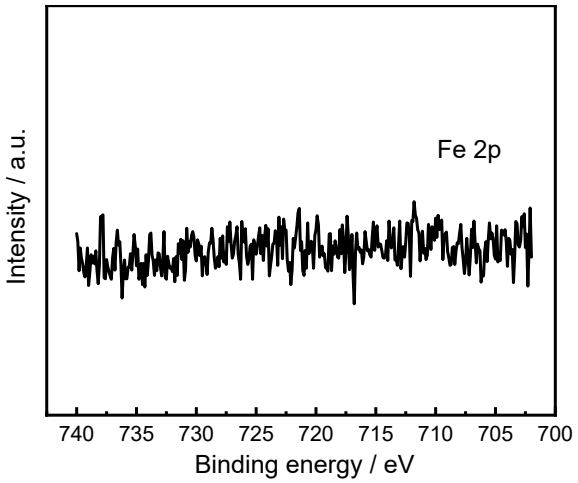

Figure S2. High-resolution Fe 2p core level spectrum of the 1D carbon substrate.

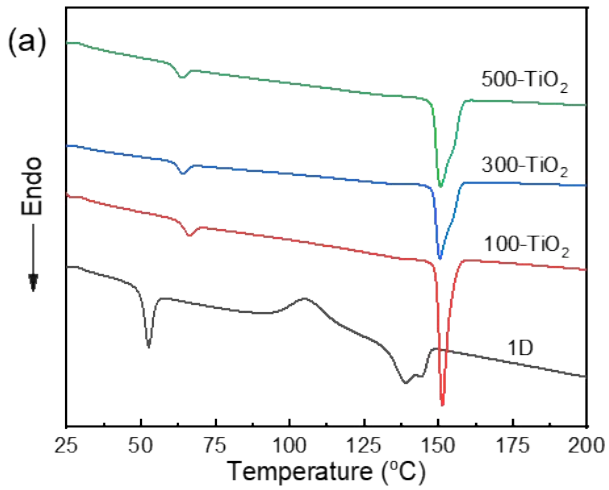

(b) The crystallinity degree evaluated by DSC

Sample	X_c (%)
1D	1.1
100-TiO_2	30.6
300-TiO_2	27.9
500-TiO_2	34.4

Figure S3. (a) DSC first heating curve of 1D carbon substrate, 100-TiO_2, 300-TiO_2, and 500-TiO_2. (b) The crystallinity degree evaluated from DSC curves in (a).

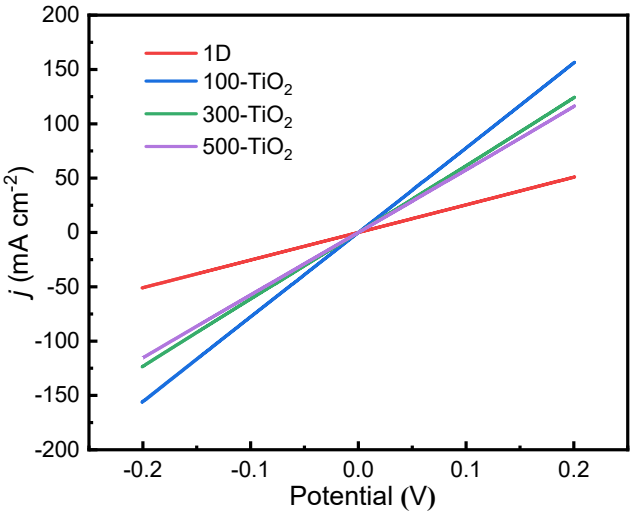

Figure S4. Conductivity test for 1D, 100-TiO_2, 300-TiO_2, and 500-TiO_2 electrodes. The electrodes are fixed between two stainless-steel rods and assembled in a Swagelok-type cell. The scan rate is 50 mV s^{-1}.

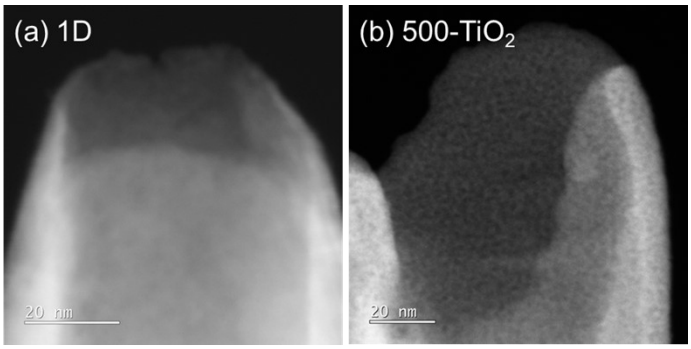

Figure S5. STEM-HAADF images of (a) 1D and (b) 500-TiO_2, showing ALD-coated TiO_2 nanoclusters on the surface of 1D carbon substrate.

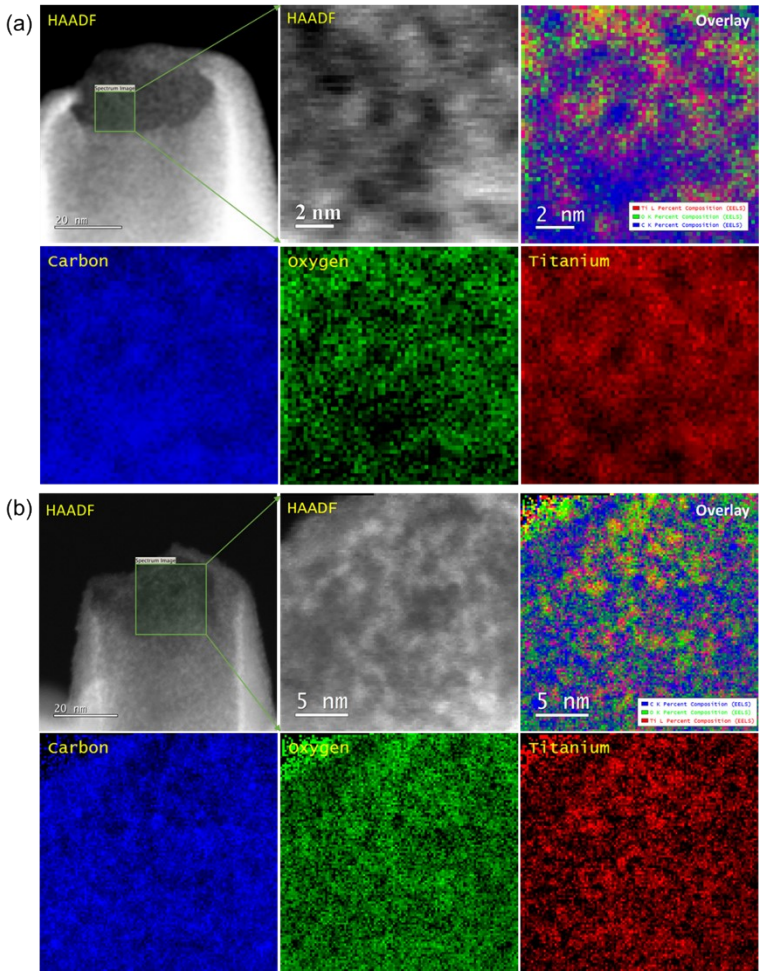

Figure S6. STEM-HAADF images of two different carbon nanotubes from 100-TiO_2 electrode, and corresponding STEM-EELS maps of C-K, O-K and Ti-L signal complemented with an overlay of all three maps.

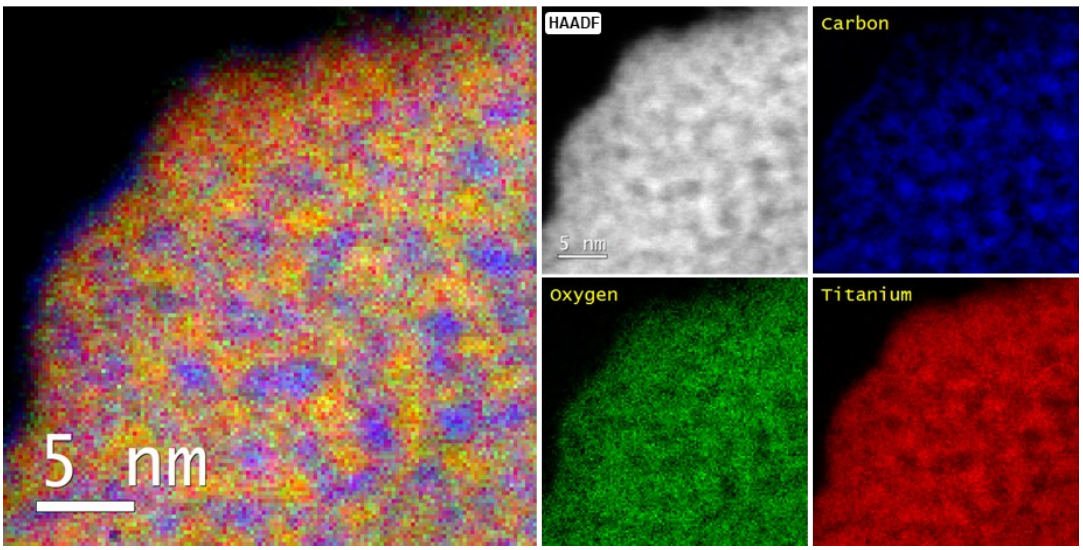

Figure S7. STEM-EELS analysis of the 500-TiO_2 electrode, showing almost continuous ALD-coated TiO_2 nanoclusters on the surface of the carbon nanotube.

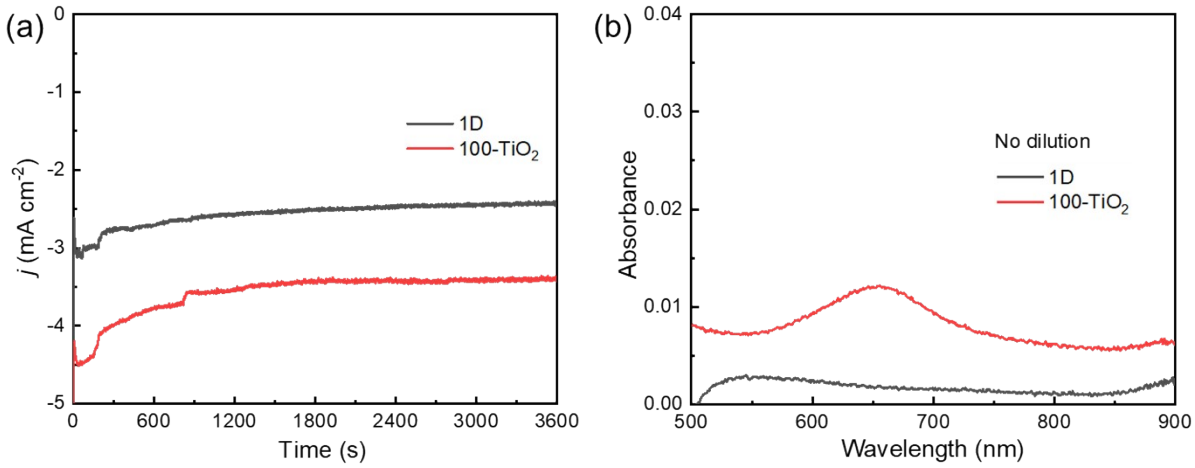

Figure S8. (a) Chronoamperometry curves of 1D and 100-TiO_2 electrodes at -1.06 V *vs*. RHE in a solution containing only 0.5 M Na_2SO_4, and (b) corresponding UV-vis absorption spectra of the electrolysis solutions.

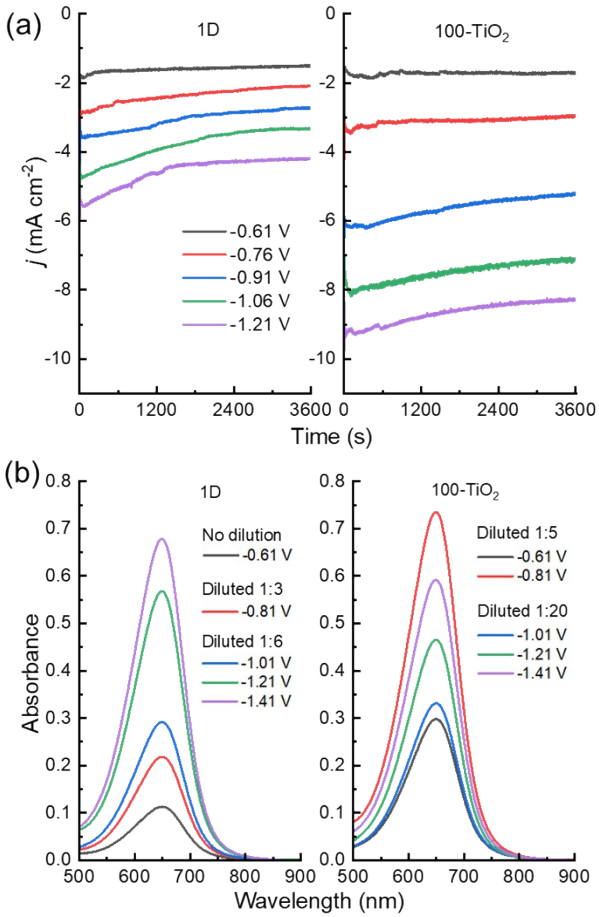

Figure S9. (a) Chronoamperometry curves of 1D and 100-TiO_2 electrodes at different potentials, and (b) corresponding UV-vis absorption spectra of the electrolysis solutions.

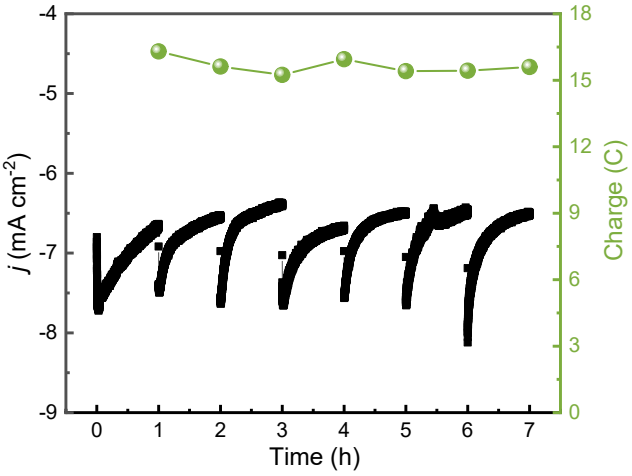

Figure S10. Current density and charge consumption for 100-TiO_2 electrode over 7 consecutive NH_3 production cycles at -1.06 V *vs*. RHE (1 hour per cycle) with refreshed electrolyte.

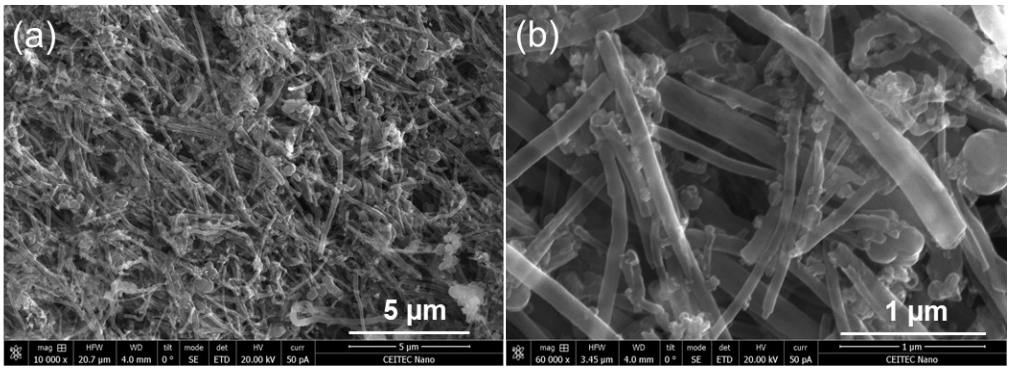

Figure S11. SEM images of 100-TiO_2 electrode after electrolysis cycling test.

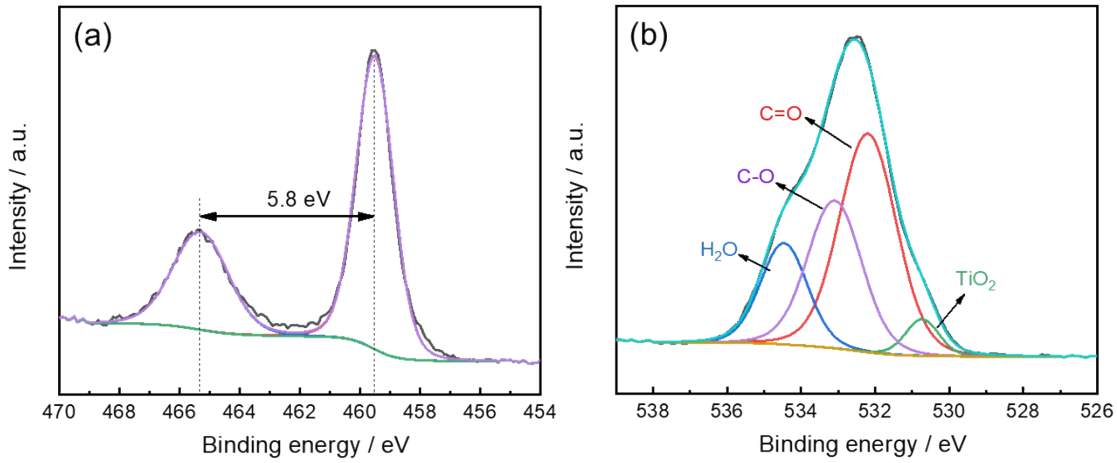

Figure S12. Ti 2p and O 1s high-resolution spectra of 100-TiO_2 electrode after electrolysis cycling test.

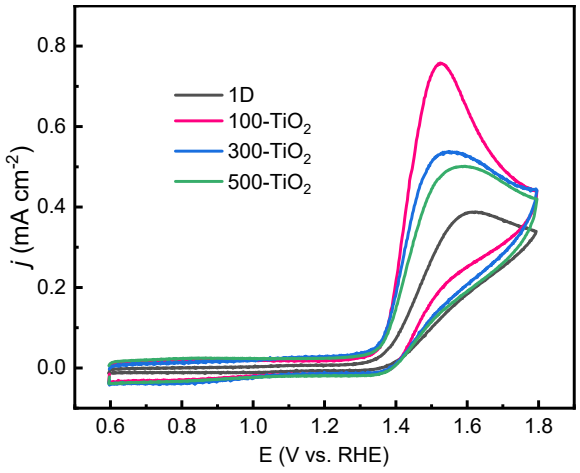

Figure S13. (a) CV curves of 1D, 100-TiO_2, 300-TiO_2, and 500-TiO_2 electrodes at 50 mV s^{-1} in the presence of 1 mM $NaNO_2$ in 0.5 M Na_2SO_4 electrolyte.

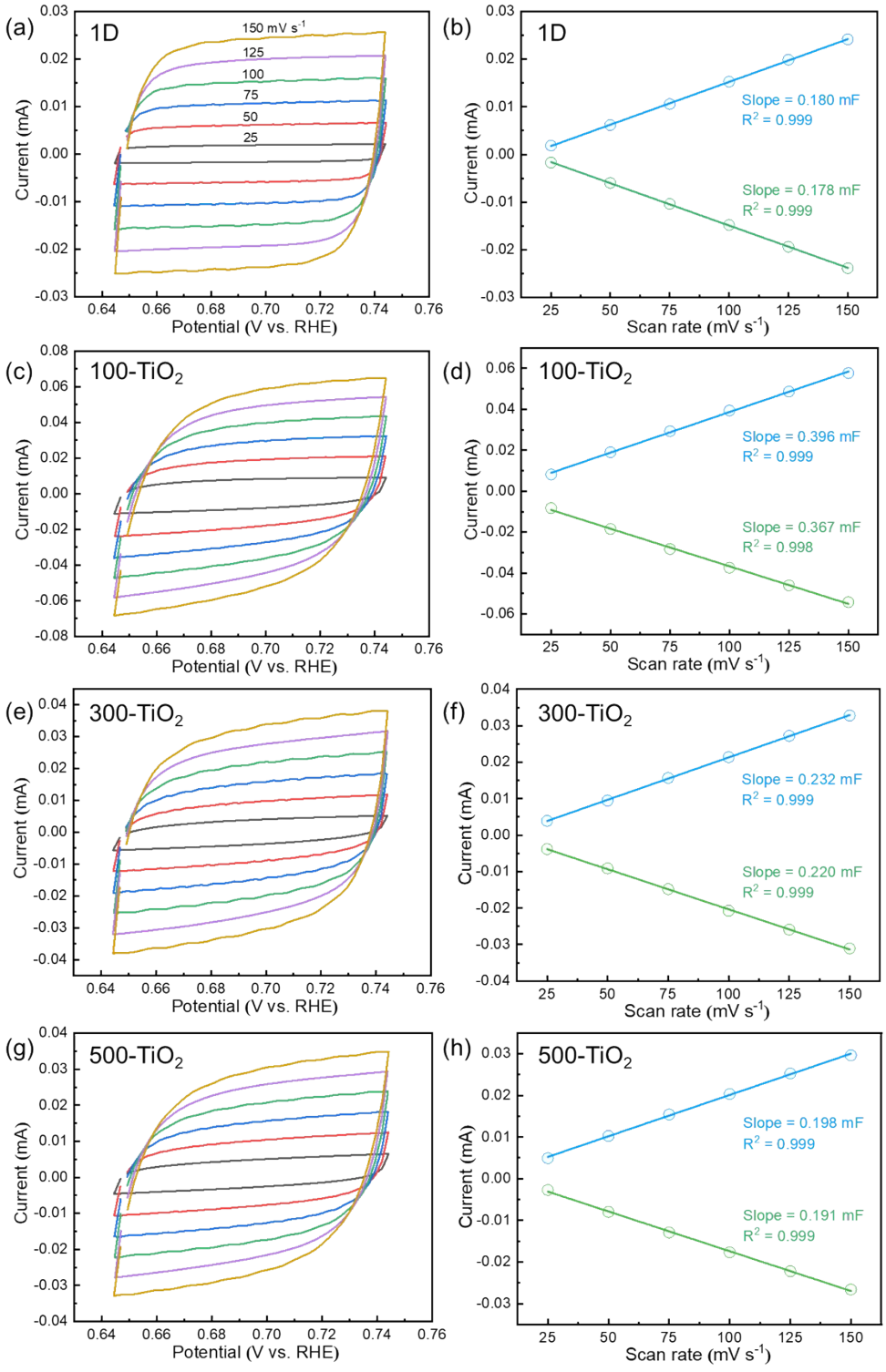

Figure S14. CV profiles of the (a) 1D, (c) 100-TiO_2, (e) 300-TiO_2, and (g) 500-TiO_2 electrode in a non-Faradaic potential region at different scan rates. (b, d, f, and h) The corresponding anodic and cathodic currents at the center of the potential window plotted as a function of scan rate to

estimate the double-layer capacitance. The calculated ECSA values of 1D, 100-TiO_2, 300-TiO_2, and 500-TiO_2 are 8.136, 17.341, 10.273, and 8.841 cm^2, respectively.

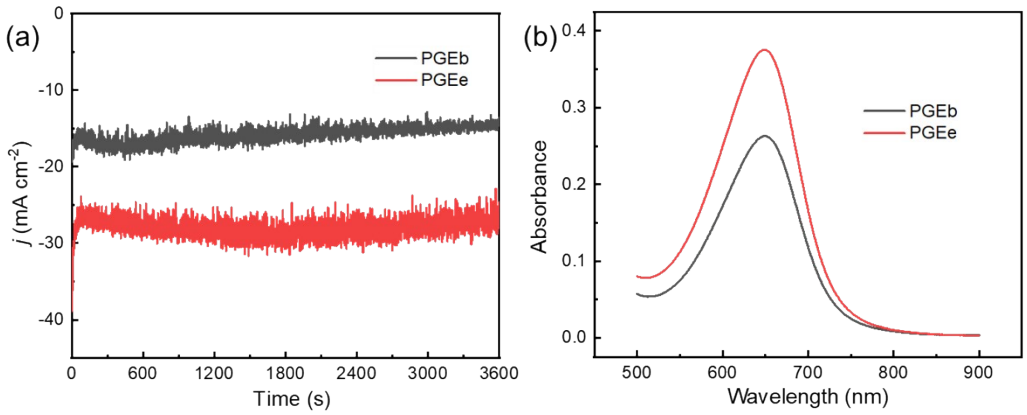

Figure S15. (a) Chronoamperometry curves of PGEb and PGEe at -1.06 V *vs*. RHE, and (b) corresponding UV-vis absorption spectra of the electrolysis solutions.

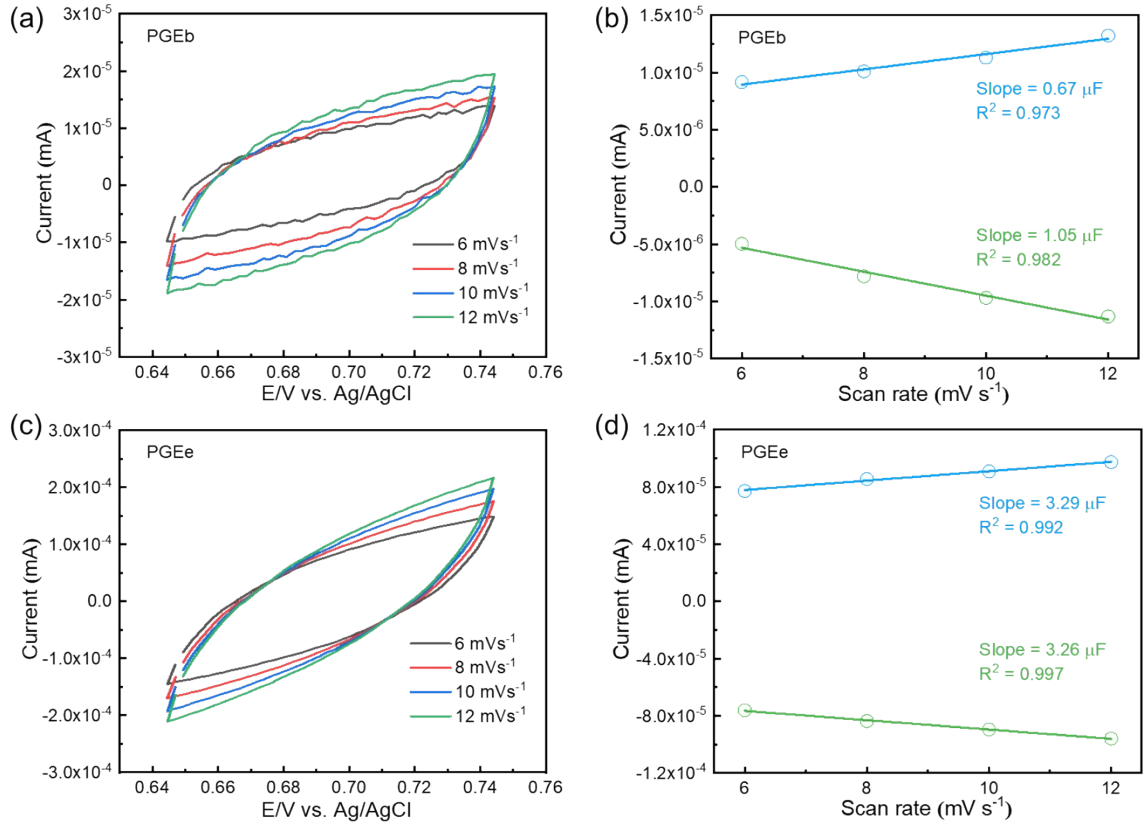

Figure S16. CV profiles of the (a) PGEb and (c) PGEe in a non-Faradaic potential region at different scan rates. (b, d) The corresponding anodic and cathodic currents at the center of the

potential window plotted as a function of scan rate to estimate the double-layer capacitance. The calculated ECSA values of PGEb and PGEe are 0.039 cm^2 and 0.149 cm^2, respectively.

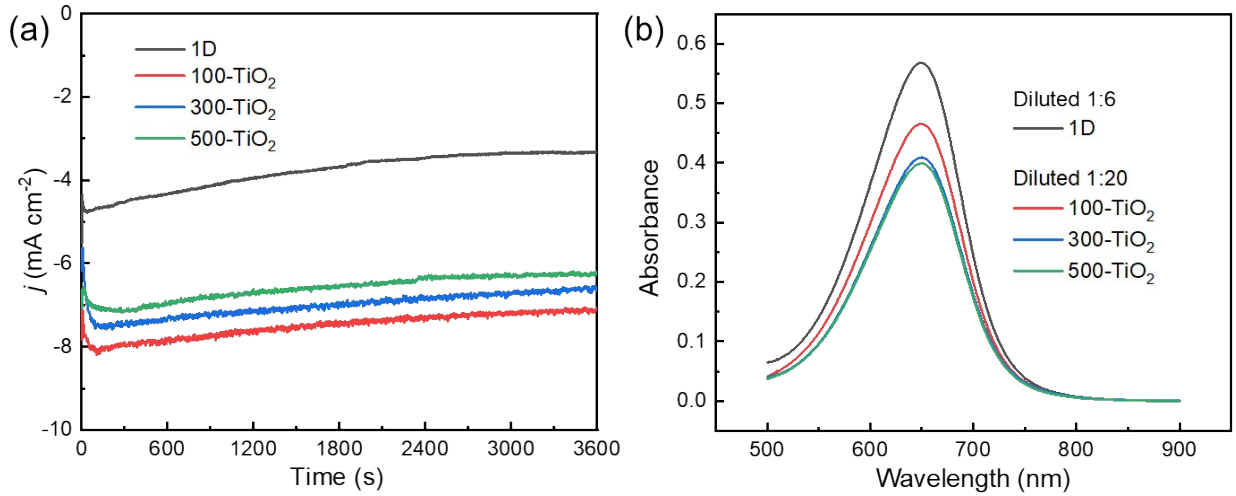

Figure S17. (a) Chronoamperometry curves and (b) corresponding UV-vis absorption spectra of electrolysis solutions of 1D, 100-TiO_2, 300-TiO_2, and 500-TiO_2 at -1.06 V *vs*. RHE.

References

[1] W. Gao, C. Iffelsberger, M. Pumera, Dual polymer engineering enables high-performance 3D printed Zn-organic battery cathodes, Appl. Mater. Today, 28 (2022) 101515, https://doi.org/10.1016/j.apmt.2022.101515.

[2] C.C. McCrory, S. Jung, J.C. Peters, T.F. Jaramillo, Benchmarking heterogeneous electrocatalysts for the oxygen evolution reaction, J. Am. Chem. Soc., 135 (2013) 16977-16987, https://doi.org/10.1021/ja407115p.